The Hydroxyl of Threonine 13 of the Bovine 70-kDa Heat Shock Cognate Protein Is Essential for Transducing the ATP-Induced Conformational Change[†,‡]

Marcelo C. Sousa and David B. McKay*

Beckman Laboratories for Structural Biology, Department of Structural Biology, Stanford University School of Medicine, Stanford, California 94305-5400

Received June 25, 1998; Revised Manuscript Received September 10, 1998

ABSTRACT: The mechanism by which ATP binding transduces a conformational change in 70-kDa heat shock proteins that results in release of bound peptides remains obscure. Wei and Hendershot demonstrated that mutating Thr37 of hamster BiP to glycine impeded the ATP-induced conformational change, as monitored by proteolysis [(1995) *J. Biol. Chem. 270*, 26670−26676]. We have mutated the equivalent resitude of the bovine heat shock cognate protein (Hsc70), Thr13, to serine, valine, and glycine. Solution small-angle X-ray scattering experiments on a 60-kDa fragment of Hsc70 show that ATP binding induces a conformational change in the T13S mutant but not the T13V or T13G mutants. The kinetics of ATP-induced tryptophan fluorescence intensity changes in the 60-kDa proteins is biphasic for the T13S mutant but monophasic for T13V or T13G, consistent with a conformational change following initial ATP binding in the T13S mutant but not the other two. Crystallographic structures of the ATPase fragments of the T13S and T13G mutants at 1.7 Å resolution show that the mutations do not disrupt the ATP binding site and that the serine hydroxyl mimics the threonine hydroxyl in the wild-type structure. We conclude that the hydroxyl of Thr13 is essential for coupling ATP binding to a conformational change in Hsc70. Molecular modeling suggests this may result from the threonine hydroxyl hydrogen-bonding to a γ-phosphate oxygen of ATP, thereby inducing a structural shift within the ATPase domain that couples to its interactions with the peptide binding domain.

The bovine 70-kDa heat shock protein (Hsc70)[1] is a member of a family of molecular chaperones, generally known as Hsp70s, that bind and release unstructured, hydrophobic segments of polypeptides in an ATP-dependent cycle, thereby presumably suppressing polypeptide aggregation and misfolding (*1*). Peptide binding and release is regulated by tightly bound ($K_d \sim 10^{-7}$ M) nucleotide; MgADP stabilizes a complex of Hsc70 with a peptide, while binding of MgATP induces a conformational change in Hsp70s that destabilizes the complex so that the peptide is released. Fluorescence (*2*−*6*), proteolysis (*3*, *7*−*9*), circular dichroism (*10*), and solution small-angle X-ray scattering (SAXS) studies (*11*, *12*) have provided evidence for the ATP-dependent conformational change in Hsp70 proteins. The ATPase and peptide binding activities of Hsp70s lie in two functionally and physically separable domains, and representative structures of both an amino-terminal ATPase domain (residues 1−386 of bovine Hsc70) (13) and a carboxy-terminal peptide binding domain (residues 389−607 of *Escherichia coli* DnaK) (*14*) have been determined. However, the interactions between the two domains and the molecular mechanism by which ATP binding transduces a structural transition between them is still not understood.

Using proteinase K digestion patterns to monitor nucleotide-dependent conformations of hamster BiP, Hendershot and co-workers constructed an "ATP-induced conformation" mutant in which ATP bound tightly but did not induce a conformational change from the ADP-bound state (*9*). The mutation, T37G, lies in the nucleotide binding cleft of the molecule, and the investigators suggested that this residue is involved in coupling ATP binding with peptide release.

To further explore the suggestion put forth by Hendershot and co-workers, we have mutated the equivalent threonine residue in Hsc70 to glycine (T13G), serine (T13S), and valine (T13V) and have analyzed how the mutations affect the coupling of ATP binding to a conformational change. Previous SAXS studies have demonstrated that a 60-kDa fragment (residues 1−554) of Hsc70 undergoes an ATP-induced conformational change that is similar in magnitude and kinetics to that observed with full-length Hsp70, while at the same time the fragment is more amenable to solution

† This work was supported by Grant GM-39928 from the National Institutes of Health to D.B.M., a Human Frontier Science Program Fellowship to M.C.S., and Proposal 2240 at the Stanford Synchrotron Radiation Laboratory (SSRL). Operation of beamline 4-2 at SSRL is supported by the Department of Energy, Office of Basic Energy Sciences, Division of Chemical Sciences. Additional support to SSRL is provided by the NIH National Center of Research Resources Biochemical Research Technology Program (RR-01209), Division of Research Resources, and by the Department of Energy, Office of Health and Environmental Research.

‡ Coordinates have been deposited in the Brookhaven Protein Data Bank, accession numbers 1bup and 2bup for the T13S and T13G mutants, respectively.

* To whom correspondence should be addressed.

[1] Abbreviations: Hsc70, 70 kDa heat shock cognate protein; Hsp70, 70 kDa heat shock protein; HEPES, *N*-(2-hydroxyethyl)piperazine-*N*′-2-ethanesulfonic acid; MOPS, 3-(*N*−morpholino)propanesulfonic acid; CHES, 2-(N−cyclohexylamino)ethanesulfonic acid; PEG-8000, poly(ethylene glycol) of approximate molecular weight 8000; SAXS, solution small-angle X-ray scattering.

10.1021/bi981510x CCC: $15.00
Published on Web 10/16/1998

studies because it is not prone to self-aggregation (*11*, *15*). Hence, this 60-kDa fragment is a convenient mimic of Hsc70 for studies of the coupling mechanism of the protein. In this context, we have used solution scattering, stopped-flow fluorescence, X-ray crystallographic, and ATPase kinetic studies to determine the effect of mutations of Thr13 on the ATP-induced conformational change of a 60-kDa fragment of Hsc70 and, by implication, to determine the participation of the hydroxyl and methyl groups of the threonine side chain in the mechanism of coupling ATP binding to a structural transition in Hsc70.

EXPERIMENTAL PROCEDURES

Mutagenesis. Mutations were introduced into the coding sequence for the 44-kDa ATPase fragment of bovine Hsc70 in an expression vector described previously (*16*). Mutagenesis was done using reagents and protocols of the Muta-Gene kit from Bio-Rad. The mutagenic oligonucleotides were of the form 5′-CCCACACAAGAATAGGT*NNN*GC-CAAGATCAATGCC, where *NNN* = GCT for T13S, AAC for T13V, and GCC for T13G. The presence of the correct mutation was confirmed in each case by dideoxy DNA sequencing of 150−200 bases spanning the mutated region. Mutations were transferred to expression vectors for both wild-type and E543K mutant 60-kDa fragments of Hsc70 by transferring restriction fragments spanning most of the ATPase coding sequence (between *Nde*I and *Nar*I sites) to these vectors, yielding expression constructs for proteins having one (T13S, T13V, and T13G) or two (T13S + E543K, T13V + E543K, and T13G + E543K) mutations.

Expression and Purification of Mutant Proteins. Mutant proteins were expressed in *E. coli* as described (*16*, *15*). Both the 44-kDa and the 60-kDa fragments were purified by ion exchange with Q-Sepharose and affinity chromatography with ATP−agarose using gravity-flow columns, followed by chromatofocusing with Mono-P and gel filtration with Superdex-75 FPLC columns (Pharmacia Biotech Inc.). Proteins were stored in 10 mM MOPS/100 mM KOAc at −70 °C.

Solution Small-Angle X-ray Scattering (SAXS). Small-angle X-ray scattering data were measured on beamline 4-2 of the Stanford Synchrotron Radiation Laboratory (SSRL) with the resident camera and one-dimensional position sensitive proportional counter (BioLogic, Grenoble, France) as described previously (*11*). Sample cell temperature was controlled at 20 °C, and solutions contained 40 mM HEPES, 150 mM KCl, 4.5 mM $MgCl_2$, 5 mM β-mercaptoethanol, and 0.5 mM nucleotide (ADP or ATP), pH 7.0. Protein concentration was 2−7 mg/mL. To avoid X-ray damage, exposure to the beam was limited to 20 min for each sample. Radii of gyration (R_g) were computed with the Guinier approximation (*17*) using the ANOM program suite (*18*), and pair distribution functions were computed using the GNOM program suite (*19*) as published previously (*11*).

ATP Hydrolysis. Rate constants for ATP hydrolysis by the 60-kDa fragments were determined under single turnover conditions at 25 °C as described previously (*20*). Briefly, 2−4 μM protein were incubated with 10 nM [α-^{32}P]ATP (10mCi/mL; 3000 Ci/mmol from Amersham) in a buffer containing 40 mM HEPES, 150 mM KCl, and 4.5 $MgCl_2$, pH 7.0. For the T13*x* mutants (*x* = S, V, G), the time course of the reaction was followed by direct spotting of 1-μL aliquots on a PEI−cellulose F TLC plate that was immediately developed with neat methanol, air-dried, and then developed with 0.5 M LiCl/1.0 M formic acid. In the case of wild-type protein, reactions were stopped by quenching with 10% TCA, neutralized, and then analyzed by spotting on the TLC plates as described above.

The extent of hydrolysis was measured by quantitating, for each time point, the radioactivity in both ADP and ATP spots after exposing the TLC plates to a phosphorimager screen. The hydrolysis rate constant was calculated by fitting a single exponential to the data on fraction of ATP hydrolyzed versus time.

Fluorescence Measurements. Measurements of the change of intensity of tryptophan fluorescence induced by MgATP binding were carried out in 40 mM HEPES buffer, pH 7.0, containing 75 mM KCl and 4.5 mM $Mg(OAc)_2$ at 18 °C in a manner described previously (*4*). The final protein concentration was 2.5 μM, and the ATP concentration ranged from 20 to 360 μM. The kinetic experiments were performed on a Bio DX-17MV stopped-flow ASVD spectrofluorometer (Applied Photophysics Ltd., Leatherhead, U.K.) equipped with a 150 W xenon arc lamp. The excitation wavelength was set to 290 nm (1 nm slit width), and the tryptophan fluorescence was selected with a SWG305 cutoff filter (CVI Laser, Albuquerque, NM). The experiments were initiated by rapid mixing of equal volumes of protein solution and nucleotide solution, and the time course of the change in flourescence was recorded. The instrument time constants used for the fast ($\leq$0.2 s) and slow phase ($20 \leq x \leq 200$ s) of the reaction were 0.15 and 1 ms, respectively. To determine a rate constant for the initial change in fluorescence intensity (k_α), a single exponential was fit to data in the range of 0.0−0.2 s. In cases where the time dependence of the fluorescence change was biphasic, a single exponential was independently fit to data over the time range of 1.0−20.0 s to determine the rate constant (k_β) of the second kinetic phase.

Determination of the Equilibrium Binding Constant for MgATP. The equilibrium dissociation constant (K_d) for complexes of mutant 60-kDa protein and MgATP were measured using a filter binding assay (*21*). Solutions of protein were mixed with [α-^{32}P]ATP in 40 mM HEPES buffer, pH 7.0, containing 75 mM KCl and 4.5 mM $Mg(OAc)_2$ at a temperature of 18 °C in a total volume of 20 μL. The nucleotide concentration was kept fixed at 2 nM, and the protein concentration ranged from 0.125 to 4.5 μM. BA-85 nitrocellulose filters (Schleicher and Schuell) were prewashed with water and reaction buffer. After being incubated for 2 min, 15 μL of the reaction mixture was spotted in the filters and immediately washed with 1 mL of reaction buffer. The filters were then air-dried, and the bound radioactivity was measured by Cerenkov radiation using a Beckman LS 5000TA scintillation counter. The function $F = F_{max}[P]/([P] + K_d)$ was fit to the values of amount of ATP bound (=F) versus protein concentration (=[P]) to give a value for K_d.

Crystallization and Data Collection. Mutant ATPase fragment proteins were crystallized at 4 °C by vapor diffusion in the presence of 1 mM MgATP, 50 mM CHES (pH 9.0), 1 M KCl, and 20% PEG-8000. Crystallization droplets were first seeded with small crystals of wild-type protein. After these crystals had grown more than 100 times their original

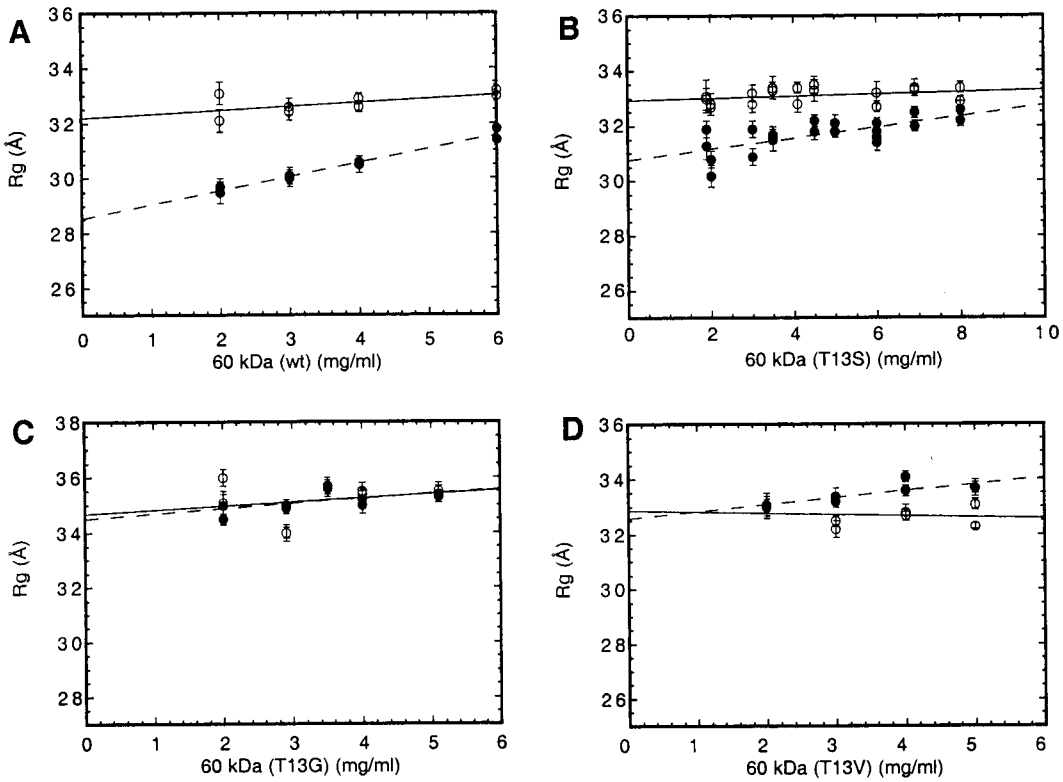

FIGURE 1: Steady-state values of R_g, computed by Guinier approximation, versus protein concentration for 60-kDa fragment proteins. (A) Wild type, reported previously and included here for comparison (*15*), (B) T13S, (C) T13G, and (D) T13V. (○) in the presence of MgADP; (●) in the presence of MgATP. The error bars represent the standard deviation of the least-squares fitting of the data in the Guinier region. Solid and dashed lines represent the linear fit of the data in the presence of MgADP and MgATP, respectively.

Table 1: Values of R_g from Solution Small-Angle Scattering Measurements

amino acid at position 13	single mutant T13*x*			double mutant T13*x*/E543K		
	ADP	ATP	ΔR_g[a]	ADP	ATP	ΔR_g[a]
T (wild type)	32.2 (±0.3)[b]	28.6 (±0.1)[b]	−3.6 (±0.3)	31.8 (±0.4)	28.8 (±0.5)	−3.0 (±0.6)
S	32.9 (±0.2)	30.8 (±0.2)	−2.1 (±0.3)	32.8 (±0.3)	28.3 (±0.3)	−4.5 (±0.4)
G	34.7 (±0.1)	34.5 (±0.2)	−0.2 (±0.2)	31.1 (±0.3)	30.8 (±0.3)	−0.3 (±0.4)
V	32.9 (±0.4)	32.6 (±0.3)	−0.3 (±0.5)	32.7 (±0.6)	31.9 (±0.7)	−0.8 (±0.9)

[a] $\Delta R_g = R_g(\text{ATP}) - R_g(\text{ADP})$. Values of R_g are extrapolations to zero protein conentration from values determined at several concentrations using the Guinier approximation. [b] Reported previously and included for comparison (*15*).

volume, they were broken into pieces and used for seeding new droplets, thereby reducing the presence of wild-type protein present in the crystals to a negligible amount. The crystals were then adapted to a cryosolvent (50 mM CHES (pH 9.0), 1 M KCl, 20% PEG-8000, and 20% ethyleneglycol) by successive 10-min soaks in solutions containing increasing amounts of ethylene glycol (5, 10, 15, and 20%). Crystals were then flash-frozen to 100 K in a stream of cold N_2 gas. Data were collected with a Rigaku R-IIC image plate system using copper K_α radiation. Data collection and processing were done as described in ref *22*.

Model Refinement. The program CNS was used for model refinement by positional retrained minimization using the maximum likelihood target function (*23*). Model building was done with the program O (*24*). Other crystallographic computations were done using the CCP4 program package.

RESULTS

Solution Small-Angle X-ray Scattering. Earlier SAXS experiments have demonstrated that ATP binding induces a measurable decrease in radius of gyration (ΔR_g) in wild-type 60-kDa fragment protein (*11*, *15*); the most plausible explanation for the ΔR_g is that it monitors the ATP-induced conformational change that results in peptide release in Hsp70 proteins (as discussed in ref 11). The 60-kDa fragment is particularly amenable to SAXS experiments since it does not self-aggregate, in contrast to full-length wild-type Hsc70 for which rapid sample oligomerization interferes with steady-state scattering measurements. Hence, to determine whether ATP induces a similar conformational change in the T13*x* mutant 60-kDa fragment proteins, steady-state values of R_g were measured in the presence of ADP and ATP.

Plots of R_g (computed in the Guinier approximation) versus protein concentration wild-type and the three mutant proteins are shown in Figure 1, and extrapolated values of R_g at zero protein concentration are summarized in Table 1. It is apparent that ATP induces a significant change in R_g for the wild-type and T13S proteins but not for the T13V or T13G proteins. This conclusion is also supported by comparisons of computed pair distribution curves that include data to a higher angle than the Guinier approximation, which shows

Table 2: ATP Hydrolysis Rates at 25 °C of Wild-Type and Mutant 60-kDa Fragment Proteins

	hydrolysis rate (s^{-1})	
protein	[enzyme] = 4 μM	[enzyme] = 8 μM
wild type	0.0048 (±0.0004)	not measured
T13S	0.00043 (±0.00001)	0.00043 (±0.00002)
T13V	0.000073 (±0.000001)	0.000085 (±0.000004)
T13G	0.0000105 (±0.0000001)	0.0000101 (±0.0000001)

a transition from an elongated molecule with ADP to a more compact structure with ATP only for the wild-type and T13S mutant proteins (data not shown).

Earlier experiments have additionally demonstrated a similar ATP-induced ΔR_g in Hsc70 and 60-kDa fragment proteins having an E543K mutation in the peptide binding domain (*11*). As further confirmation of the effects we see with the single point mutations at residue 13, we have measured SAXS data on double mutant proteins (T13S/E543K; T13G/E543K and T13V/E543K) and compared the results to the E543K 60-kDa fragment. We observe a similar pattern in the double mutants; T13S/E543K undergoes the ATP-induced ΔR_g, while T13G/E543K and T13V/E543K do not. Thus, both for single mutations and in the context of the secondary E543K mutation, the presence of a hydroxyl group (from theonine or serine) is required at position 13 for the ΔR_g that is indicative of an ATP-induced conformational change.

Rate Constants of ATP Hydrolysis. The transition to the smaller R_g state in Hsc70 and its 60-kDa fragment is predicated on ATP binding, while the reverse transition to the larger R_g state requires product release (*25*, *11*). In a steady-state SAXS experiment (i.e., when nucleotide is present in large molar excess over protein), the observed decrease in R_g is dependent on both the magnitude of the conformational change and the fraction of time during the overall ATPase cycle that the protein has (unhydrolyzed) ATP bound. Hence, an alternative explanation for not observing an ATP-induced ΔR_g in a mutant protein would be that the ATP hydrolysis rate is substantially faster than that of wild-type protein. In this context, we have measured the single-turnover ATP hydrolysis rate for each of the mutant 60-kDa fragments and have compared it to the value for wild-type protein. Reactions were followed to completion, where [α-^{32}P]ADP accounted for 90% ± 10% of the total counts, with the residual counts being due to nonspecific background. The hydrolysis constants were calculated by fitting a single exponential to data on fraction of ATP hydrolyzed versus time. The results obtained for the three 60-kDa T13x mutant fragments at 4 and 8 μM protein concentrations are shown in Table 2. For each mutant, values measured at the two different protein concentrations are equal within $\pm 2\sigma$ error, showing that the substrate is saturated with enzyme under these conditions, as anticipated if the K_m for ATP is not dramatically higher than the ~0.1 μM value observed for wild-type Hsc70 protein and T37G mutant BiP. For comparison, the rate obtained for the wild-type 60-kDa protein at 4 μM enzyme concentration is also included. Although we have no direct measure of stability of these particular 60-kDa proteins, we note that we have crystallized both wild type and several mutants of the 60-kDa protein (data not shown), which requires the structural integrity of the protein over a period of several days, so that the slow hydrolysis rates we observe are unlikely to be the result of protein denaturation.

It can be seen that the hydrolysis rate constant for the T13S mutant protein is 1 order of magnitude slower that that of wild-type protein, while the T13V and T13G proteins are approximately 2 orders of magnitude slower, with the activity of T13G protein being barely detectable. These data demonstrate that ATP hydrolysis is severely impaired in absence of a hydroxyl group at position 13 and confirm that the disappearance of the ATP-induced ΔR_g in steady-state SAXS experiments is due to abolition of the intramolecular conformational change rather than to alteration of ATPase cycle kinetics.

ATP-Induced Changes in Fluorescence. Previous work on Hsc70 E543K protein and its 60- and 44-kDa fragments demonstrated that binding of MgATP induces a change in the intrinsic tryptophan fluorescence intensity (*4*). Under conditions where MgATP binding induces a measurable decrease in R_g in Hsc70 and its 60-kDa fragment (interpreted as a conformational change), the fluorescence change has both a rapid and a slow kinetic step. The rate constant of the rapid step increases linearly with ATP concentration, as expected for a bimolecular association process; the rate constant of the slow step is constant for sufficiently high ATP concentrations, suggestive of an intramolecular conformational rearrangement. The second, slow step does not occur under conditions where nucleotide binding fails to induce a conformational change (e.g., binding of MgADP or MgAMPPNP). These data support a model in which the MgATP-induced conformational change in Hsc70 and its 60-kDa subfragment occurs as a second, kinetically separable step after initial nucleotide binding.

We have carried out stopped-flow fluorescence measurements on a subset of the 60-kDa proteins used in these studies; the results are summarized in Table 3. For wild-type, T13S, and T13S/E543K proteins, the fluorescence intensity change induced by MgATP binding displays two kinetic phases. The rate constant of the first phase is linearly dependent on [ATP], while the rate constant of the second phase is independent of [ATP]. With the T13V and T13G mutant proteins, we do not see a second phase in the fluorescence intensity change; only the initial, rapid phase is observed. This correlates with the prediction from the SAXS results; the T13V and T13G mutants cannot undergo a MgATP-induced conformational change, while the T13S mutant does.

The observed rate constants of the fluorescence intensity change (denoted k_α and k_β for the rapid and slow phase, respectively) can be interpreted with the two-step Scheme 1 that has been presented and justified previously (*4*), in which initial nucleotide binding (the rapid phase) is followed by a conformational change (the slow phase), where E represents the large R_g, nucleotide-free form of a 60-kDa protein and E* represents the small R_g form after the ATP-induced conformational change. [The nomenclature of $k_{\pm 1}$ and $k_{\pm 1}$* is used for consistency with previous papers, where k_2 has been used to denote the rate of ATP hydrolysis (*20*, *4*).] The slope of a linear fit of k_α versus [ATP] is equal to k_1; the intercept is equal to ($k_{-1} + k_1^* + k_{-1}^*$). For the ATP concentrations used in these experiments, k_β is constant and equal to $k_1^* + k_{-1}^*$. The measured values of k_β are much smaller than the corresponding values of the intercept of the

Table 3: Rate and Equilibrium Binding Constants for ATP

protein	$10^5 k_1$ (M^{-1} s^{-1})[a]	k_{-1} (s^{-1})[b]	k_β (s^{-1})	K_d (μM)	computed $K_d^1 = k_{-1}/k_1$ (μM)	computed $K_d^* = k_{-1}^*/k_1^*$
wild type	4.3 (±0.4)	0.6 (±2.3)	0.0601 (±0.0009)	nd[c]	1.4 (±5.4)	nd
T13S	6.6 (±0.1)	2.0 (±0.6)	0.0303 (±0.0002)	3.0 (±1.0)	3.0 (±0.9)	1.0 (±0.6)
T13S/E543K	6.6 (±0.2)	1.7 (±0.8)	0.02463 (±0.00008)	1.0 (±0.1)	2.6 (±1.2)	0.4 (±0.2)
T13V	1.95 (±0.05)	nd	not observed	nd	nd	nd
T13G	1.59 (±0.08)	nd	not observed	nd	nd	nd
E543K	4.7[d]	nd	0.14[d]	nd	nd	nd

[a] Calculated from slope of k_α versus [ATP] from fluorescence data. [b] Calculated from intercept of k_α versus [ATP]. [c] nd, not determined. [d] Values estimated for 18 °C from data published previously (*4*).

Scheme 1

$$E + ATP \underset{k_{-1}}{\overset{k_1}{\rightleftharpoons}} E\text{–}ATP \underset{k^*_{-1}}{\overset{k^*_1}{\rightleftharpoons}} (E\text{–}ATP)^*$$

linear fit of k_α versus [ATP] in each case measured here, so that the intercept is essentially equal to k_{-1}. Values of kinetic constants derived from these data are summarized in Table 3. For comparison, the values for the E543K 60-kDa fragment, extrapolated to 18 °C from data measured previously (*4*), are included in Table 3.

Equilibrium Binding of ATP. To further quantify the ATP association reaction for the T13S and T13S/E543K mutants, the equilibrium binding constant for ATP was measured using the filter binding assay described in Materials and Methods. This method requires that the rate at which ATP binds and induces a conformational change is rapid as compared to the rate of ATP hydrolysis, thereby providing a time window for sampling during which the binding has essentially reached equilibrium but no significant hydrolysis has occurred. For the T13S mutants, k_1[protein] is ~0.08 s^{-1} for 0.125 μM protein and $k_\beta \sim 0.03$ s^{-1}, while the hydrolysis rate is ~0.0004 s^{-1}, so that this condition is satisfied when samples are taken ~100 s. after mixing. It is, unfortunately, not possible to determine the ATP binding constant for wild-type and E543K protein by this method, due to their more rapid hydrolysis rate, which would result in significant hydrolysis on the time scale of the sampling. Values for K_d are summarized in Table 3.

Crystallographic Structures of Mutant ATPase Fragments. Arguably, mutations at position 13 might result in a substantial structural distortion of the nucleotide binding site of Hsc70, in which case the observed effects could not be ascribed simply to the presence or absence of a single hydroxyl at this site. To address this possibility, we have solved the structures of the 44-kDa ATPase fragments of T13S and T13G proteins.

A structure of the wild-type Hsc70 ATPase fragment refined with data to 1.7 Å resolution was used as the initial model in both structure determinations (*22*). The nucleotide, metal ions, and water molecules present in the active site were removed from the model, and residue T13 was truncated to glycine. After atomic B factors were reset to 25 $Å^2$, a cycle of rigid body refinement was performed, followed by three alternating rounds of positional and individual B factor refinement using data from 6.0 to 1.7 Å. Inspection of $F_o - F_c$ and $2F_o - F_c$ maps revealed electron density for ADP, inorganic phosphate (P_i), a Mg^{2+} ion, two K^+ ions, and several water molecules that are present in the wild-type active site. These atoms were added to each model.

For T13S, clear electron density for a serine side chain was also visible at position 13 and was therefore modeled. Three more rounds of alternating positional and individual B factor refinement were carried out. At this point, the crystallographic *R* factor was 0.208, and the free *R* factor was 0.242. A solvent mask was calculated from the atomic coordinates, and the subsequent cycles of refinement included a bulk solvent correction and an overall anisotropic B factor correction. At this point, all the available data were included, and the refinement continued with cycles of model rebuilding and positional/B factor refinement until the free and crystallographic *R* factors showed no significant improvement.

The same procedure was used for the refinement of the T13G structure. In the difference maps for T13G (contoured at 3σ), an additional positive electron density peak near the β-phosphate ADP and a negative density peak overlapping the inorganic phosphate were visible, suggesting the presence of a mixture of ATP and ADP + P_i in the active site. Two groups of atoms were defined and given partial occupancy for further refinement. Group 1 consisted of ADP, P_i, and a water molecule; group 2 contained ATP and a water molecule in a position similar to that occupied by the inorganic phosphate in group 1. The atomic B factors were reset to 25, and the occupancies were defined as 0.6 for group 1 and 0.4 for group 2. A single round of simulated torsional annealing was performed for the atoms in both groups, followed by positional refinement for the entire model. A cycle of group occupancy refinement was carried out but showed no significant improvement over the original estimates. Therefore, the 0.6 and 0.4 values were maintained. After a single round of positional and individual B factor refinement, the crystallographic and free *R* factors were 0.197 and 0.226, respectively. Further rounds of model rebuilding and positional and *B* factor refinement were performed until no significant improvement was observed. The final data collection and refinement statistics for both mutants are summarized in Table 4.

When superimposed with the wild-type structure (PDB accession 1hpm), the average rms deviation for main chain and β-carbon atoms was 0.28 Å for T13S and 0.37 Å for T13G, confirming that no major structural distortions occur in the ATPase fragment of Hsc70 as a result of the glycine or serine mutations. In this context, structure determination of the T13V mutant ATPase fragment was considered redundant and was not pursued. The structure of the ATPase active site, with the T13G mutant superimposed onto the wild-type structure, as shown in Figure 2. In this figure, the structures are barely distinguishable, including at the site of the mutation. Additionally, the interaction hydroxyl in the T13S mutant with the inorganic phosphate (not shown

Table 4: Crystallographic Data Collection and Refinement Statistics

ATPase fragment mutant:	T13G	T13S
Data Collection		
cell parameters		
a (Å)	143.35	143.57
b (Å)	64.30	64.16
c (Å)	46.23	46.24
max resolution (Å)	1.70	1.70
observations	167 988	143 963
unique reflections	46 807	46 672
completeness (99.0−1.70)	0.974	0.974
completeness (1.76−1.70)	0.895	0.908
R_{sym}[a] (99.0−1.70)	0.058	0.044
R_{sym}[a] (1.76−1.70)	0.140	0.142
Refinement		
final resolution in refinement[c]	100.0 − 1.7	100.0 − 1.7
reflections used in working set	42 106	42 013
reflections in test set	4 701	4 659
$R_{crystallographic}$[b] (100.0−1.70)	0.196	0.189
R_{free}[b] (100.0−1.70)	0.224	0.220
$R_{crystallographic}$[b] (1.71−1.70)	0.237	0.238
R_{free}[b] (1.71−1.70)	0.297	0.299
water molecules modeled	435	431
rms[d] bond deviation (Å)	0.009	0.01
rms[d] angle deviation (deg)	1.66	1.74

[a] $R_{sym} = \sum|I_i - \langle I\rangle|/\sum\langle I\rangle$ where I is the diffraction intensity; $\langle I\rangle$ is the mean measured intensity. [b] $R_{crystallographic} = \sum|F_c - F_o|/\sum F_o$ where F_o is the observed structure factor amplitude in working set $= |I^{1/2}|$; F_c is the structure factor amplitude calculated from model; R_{free} same, using F_o in test set. [c] Lowest resolution of reflections actually measured was ∼30 Å. [d] rms, root-mean-square.

in Figure 2) mimics that of the Thr13 hydroxyl. The crystallographic data argue that the effects of the mutations are due to the change of side chain functional groups at position 13, not to disruption of the tertiary structure.

DISCUSSION

Previous studies on Hsp70 proteins have shown that binding of MgATP induces a conformational change that can be modeled as the peptide binding domain "condensing" onto the ATPase domain (*11*). Presence of K^+ at ∼100 mM is required for the conformational change, and other monovalent ions such as Na^+ will not substitute, revealing a precise geometric constraint on the cation bound at the two monovalent ion binding sites of the ATPase domain (*22*, *26*). The counterion is not important; ATP induces the conformational change equally well in the presence of Cl^- or OAc^- (*11*). The interaction between domains in the condensed state releases (or more precisely, increases the "off" rate of) bound peptides; it also inhibits the ATP hydrolysis reaction, which may rely on localized structural rearrangment in the ATP binding domain after the conformational change (*15*). Previous work has also characterized a mutation in the peptide binding domain, E543K, which weakens peptide binding and also destabilizes interdomain communication by imparing the inhibition of ATP hydrolysis after the ATP-induced conformational change (*15*). The molecular mechanism by which binding of ATP in one domain transduces a signal to the other domain that results in a large interdomain structural change is unknown; the mechanism by which the E543K mutation impairs this coupling is also unknown. The interaction of Thr13 with ATP is an essential component of this mechanism.

Participation of Thr13 in Transducing a Conformational Change. Our experiments demonstrate that mutation of Thr13 to valine or glycine in the 60-kDa fragment of Hsc70 abolishes both the steady-state, ATP-induced ΔR_g measured by SAXS and the second phase of the pre-steady-state change in tryptophan fluorescence intensity that are observed in wild-type and T13S mutant proteins. These effects are not due to alterations in the kinetic constants of the ATPase cycle or to major structural distortions of the ATP binding domain. We interpret these results to demonstrate that the hydroxyl group of Thr13 participates directly in coupling ATP binding to a conformational change in Hsc70. This interpretation relies on the assumption that the coupling mechanism is fundamentally the same in the 60-kDa subfragment that lacks ∼100 carboxy-terminal amino acids that mediate intermolecular oligomerization as it is in the full-length Hsc70 protein. We have previously presented evidence to justify this assumption for the bovine Hsc70 protein (*11*); additionally, other investigators have demonstrated that a similar ∼60-kDa truncation of *E. coli* DnaK retains its ability to undergo an ATP-induced conformational change (*3*).

The results presented here for the bovine Hsc70 system corroborate the conclusions of Wei and Hendershot from experiments on hamster BiP that Thr13 (Thr37 in BiP) is essential for coupling ATP binding to a conformational change (*9*). The fact that the two sets of experiments relied on different probes of conformational change (proteolysis of BiP versus SAXS and fluorescence for a subfragment of Hsc70) and two different Hsp70 proteins argues in favor of the generalization of this conclusion to the entire Hsp70 protein family. Additionally, the results reported here demonstrate the specific requirement for a hydroxyl group at this amino acid position.

It is apparent that a hydroxyl group at residue 13 is necessary but not sufficient for wild-type behavior of Hsc70. Although the T13S mutant protein retains the coupling between ATP binding and a conformational change, its hydrolysis rate is impaired relative to wild-type protein. It is notable in this context that threonine is strictly conserved at this position in more than 100 Hsp70 protein sequences (e.g., SwissProt release 34.0, April 1996), strongly arguing for a strict functional requirement of both the hydroxyl and the methyl group of the threonine side chain. It is parenthetically notable that actin, a close structural homologue of the Hsc70 ATPase fragment, has serine rather than threonine at this position (*27*), fortifying the suggestion that the conservation of threonine in Hsc70 is a constraint imposed by protein function rather than by the protein tertiary fold.

We may suggest a model for how Thr13 might participate in coupling ATP binding to a conformational shift. The ATP-induced conformation arises after initial ATP binding but before hydrolysis. Modeling a pre-transition state complex with MgATP, in which the β- and γ-phosphates form a bidentate complex with the Mg^{2+} ion, suggests that the hydroxyl of Thr13 may hydrogen bond to a nonbonded oxygen of the terminal phosphate and in doing so may facilitate hydrolysis. The methyl group of Thr13 would then be in van der Waals contact with the methylene side chain of Lys71, a residue that is essential for hydrolysis and which positions the putative catalytic H_2O molecule for in-line attack on the terminal phosphate (Figure 3). Modeling such a configuration from the crystallographic structures of the ATPase fragment requires rotation of the threonine side chain and results in a significant steric clash between the Thr13

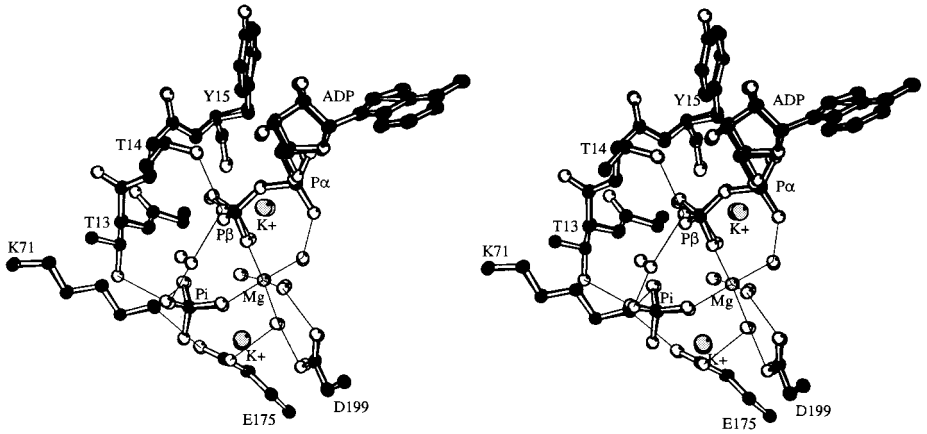

FIGURE 2: Stereoview of the T13G mutant superimposed onto the wild-type protein in the nucleotide binding region, with ADP, inorganic phosphate, selected residues, and Mg^{2+} and K^+ ions shown and labeled. Relevant water molecules are also included. Selected noncovalent interactions are shown as thin solid lines. Atoms are colored as follows: carbon, black; nitrogen and phosphorus, dark gray; oxygen, white; K^+ and Mg^{2+}, light gray. Figure made with MOLSCRIPT (*28*). The method of superposition is described in the text.

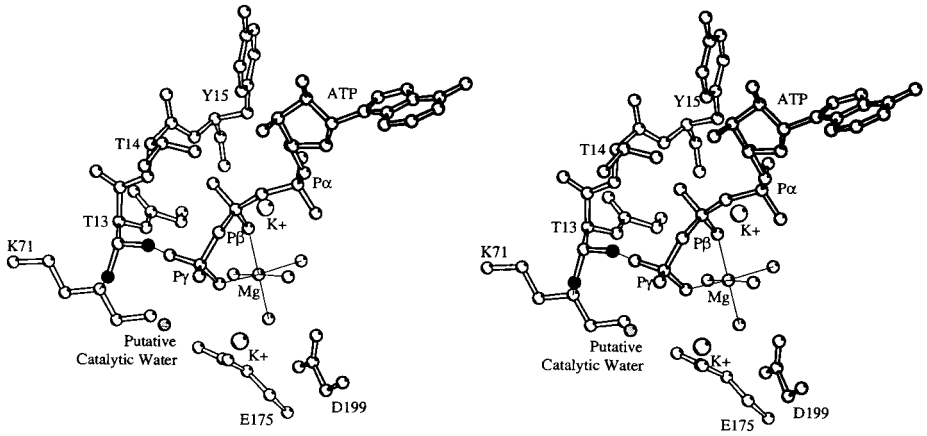

FIGURE 3: Stereo diagram of a model of a pre-transition state intermediate. Selected residues, water molecules, and a bidentate Mg^{2+}−ATP complex are shown. Noncovalent bonds are shown as fine lines. The Thr13 side chain oxygen is colored black and is shown forming a hypothetical hydrogen bond with a nonbonded oxygen of the ATP γ-phosphate; it is apparent that steric clash would result without a structural compensation. The Thr13 side chain methyl group is colored gray and is shown interacting with the methylene side chain of Lys71. The postulated catalytic water is shown and labeled. Figure made with MOLSCRIPT (*28*).

hydroxyl and the terminal phosphate of the nucleotide. It is apparent that to achieve such a configuration a subtle but significant conformational rearrangement within the ATP binding domain would be required, which in turn might be transmitted to its interface with the peptide binding domain. Thus, although we have not captured a crystallographic structure of the proposed intermediate, the hypothetical scheme we suggest to rationalize the participation of Thr13 in transducing a conformational change is plausible and consistent with available data.

Effect of a Secondary E543K Mutation in the Peptide Binding Domain. Qualitatively, the conclusions from the SAXS experiments on 60-kDa fragment proteins having single point mutations are further corroborated by experiments on proteins having a second mutation, E543K, in the peptide binding domain. Neither T13V/E543K nor T13G/E543K undergoes an ATP-induced change, while T13S/E543K does. This E543K mutation, although remote from the nucleotide, is known to destabilize both peptide binding and interdomain communication (*15*).

Quantitatively, the effects of the secondary E543K mutation can be interpreted in the framework of the two-step MgATP binding Scheme 1 (*4*). In this scheme, the overall K_d for MgATP is the product of the equilibrium constants for the two individual steps, denoted K_d^1 ($=k_{-1}/k_1$) and K_d^* ($=k_{-1}^*/k_1^*$). The overall K_d for the double mutant T13S/E543K is approximately 3-fold tighter than for the single T13S mutant. However, the values of K_d^1 for initial ATP binding for the single and double mutants, calculated from the rate constants of the early phase of stopped-flow fluorescence changes, are equal within experimental error (Table 3). From these values, we may estimate the equilibrium constant K_d^* for the conformational transition as ~1.0 for T13S and ~0.4 for T13S/E543K; the effect of the E543K mutation is seen in the second step; the ATP-induced conformational transition is energetically more favorable in the double mutant than in the single mutant. (Parenthetically, it is notable that the ΔR_g we observe by SAXS for the T13S mutant is smaller than that of the wild-type and T13S/E543K proteins; this can be understood if the equilibrium constant of the conformational transition for T13S is near unity, in which case an approximately equimolar mixture of the E and E* states would be present under the steady-state, ATP-saturated conditions of the SAXS experiment, giving rise to an R_g value that is intermediate to that of the E and E* states.)

The apparent stabilization of the ATP-induced conformation by the E543K mutation suggests the following general framework for interpreting the effects of the single and

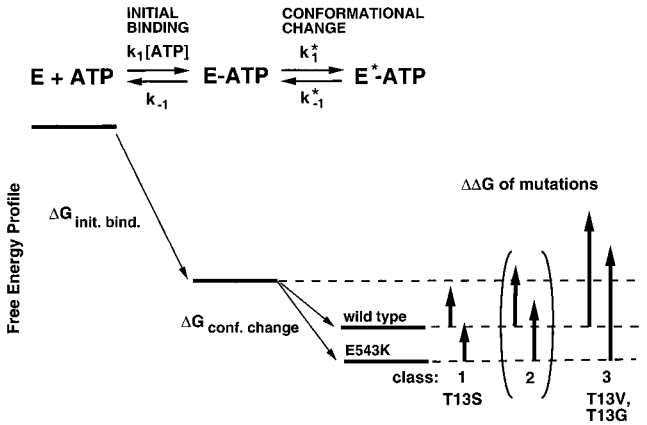

FIGURE 4: Schematic drawing of the effects of mutations on the free energy profile of ATP binding in the two-step binding scheme. Free energy differences are not drawn to scale. The effects of three prossible classes of mutations, with $\Delta\Delta G$ values represented by vertical arrows, are shown.

double mutations, drawn schematically in Figure 4. Removing the methyl group from the Thr13 side chain has a relatively small effect, so that the ATP-induced conformational change is seen in both the single T13S and double T13S/E543K proteins and is more favored in the double mutant. To the extent it is valid to approximate the effects of the mutations as independent and additive, this says that the energetic penalty to ATP binding that is introduced by the T13S mutation, denoted $\Delta\Delta G$(T13S), is approximately equal in magnitude and opposite in sign to the ΔG of the conformational transition of wild-type protein, $|\Delta\Delta G(\text{T13S})| \cong |\Delta G_{\text{conf. change}}(\text{wt})|$, resulting in a net $K_d^* \cong 1.0$ for this step, and is significantly smaller in magnitude than the ΔG of the E543K protein for this step, $|\Delta\Delta G(\text{T13S})| < |\Delta G_{\text{conf. change}}(\text{E543K})|$. This is shown schematically as class 1 in Figure 4. In contrast, removing the hydroxyl group has a much larger effect. The $\Delta\Delta G$ values of the T13V and T13G mutations are apparently larger than the ΔG of the conformational transition for both wild-type and E543K proteins, so that no conformational transition is seen in either T13V or T13G single mutant proteins or in the double mutant (T13V/E543K or T13G/E543K) proteins; these are examples of mutations of class 3 in Figure 2.

This scheme predicts an intermediate class of mutations (class 2, in parentheses in Figure 4) in which a single point mutation in the ATP binding domain abolishes the conformational transition but the secondary E543K mutation "rescues" it, $|\Delta G_{\text{conf. change}}(\text{wt})| < |\Delta\Delta G(\text{mutation})| < |\Delta G_{\text{conf. change}}(\text{E543K})|$; examples of such mutations will be presented separately (E. R. Johnson and D. B. McKay, unpublished data). The E543K mutation in the peptide binding domain therefore provides a secondary tool for segregating mutations in the ATP binding domain into three classes, based on the relative magnitudes of their effects on the mechanism of coupling ATP binding to a conformational transition in the Hsc70 protein. The third class, represented by T13V and T13G, defines the functional groups that are energetically most important for transducing the conformational change.

ACKNOWLEDGMENT

We thank Lushen Li for assistance with sample preparation; Drs. Sigurd Wilbanks, Eric Johnson, and Hiro Tsuruta for assistance with synchrotron data collection and interpretation; and Colleen Murphy for assistance with fluorescence measurements.

REFERENCES

1. Pelham, H. R. B. (1986) *Cell 46*, 959−961.
2. Palleros, D. R., Reid, K. L., McCarty, J. S., Walker, G. C., and Fink, A. L. (1992) *J. Biol. Chem. 267*, 5279−5285.
3. Buchberger, A., Theyssen, H., Schroder, H., McCarty, J. S., Virgallita, G., Milkereit, P., Reinstein, J., and Bukau, B. (1995) *J. Biol. Chem. 270*, 16903−16910.
4. Ha, J.-H., and McKay, D. B. (1995) *Biochemistry 34*, 11635−11644.
5. Banecki, B., and Zylicz, M. (1996) *J. Biol. Chem. 271*, 6137−6143.
6. Theyssen, H., Schuster, H. P., Packschies, L., Bukau, B., and Reinstein, J. (1996) *J. Mol. Biol. 263*, 657−670.
7. Liberek, K., Skowyra, D., Zylicz, M., Johnson, C., and Georgopoulos, C. (1991) *J. Biol. Chem. 266*, 14491−14496.
8. Kamath-Loeb, A. S., Lu, C. Z., Suh, W. C., Lonetto, M. A., and Gross, C. A. (1995) *J. Biol. Chem. 270*, 30051−30059.
9. Wei, J., Gaut, J. R., and Hendershot, L. M. (1995) *J. Biol. Chem. 270*, 26677−26682.
10. Banecki, B., Zylicz, M., Bertoli, E., and Tanfani, F. (1992) *J. Biol. Chem. 267*, 25051−25058.
11. Wilbanks, S. M., Chen, L., Tsuruta, H., Hodgson, K. O., and McKay, D. B. (1995) *Biochemistry. 34*, 12095−12106.
12. Shi, L., Kataoka, M., and Fink, A. L. (1996) *Biochemistry. 35*, 3297−3308.
13. Flaherty, K. M., DeLuca-Flaherty, C., and McKay, D. B. (1990) *Nature 346*, 623−628.
14. Zhu, X., Zhao, X., Burkholder, W. F., Gragerov, A., Ogata, C. M., Gottesman, M. E., and Hendrickson, W. A. (1996) *Science 272*, 1606−1614.
15. Ha, J.-H., Hellman, U., Johnson, E. R., Li, L., McKay, D. B., Sousa, M. C., Takeda, S., Wernstedt, C., and Wilbanks, S. M. (1997) *J. Biol. Chem. 272*, 27796−27803.
16. Wilbanks, S. M., DeLuca-Flaherty, C., and McKay, D. B. (1994) *J. Biol. Chem. 269*, 12893−12898.
17. Guinier, A. (1955) *Small-angle Scattering of X-rays*, John Wiley & Sons, New York.
18. Rice, M., and Wakatsuki, S. *SSRL/SLAC User Manual*.
19. Semenyuk, A. V., and Svergun, D. I. (1991) *J. Appl. Crystallogr. 24*, 537−540.
20. Ha, J.-H., and McKay, D. B. (1994) *Biochemistry 33*, 14625−14635.
21. Wilbanks, S. M., and McKay, D. B. (1998) *Biochemistry 37*, 7456−7462.
22. Wilbanks, S. M., and McKay, D. B. (1995) *J. Biol. Chem. 270*, 2251−2257.
23. Brunger, A. T., Adams, P. D., Clore, G. M., Gros, P., Grosse-Kunstleve, R. W., Jiang, J.-S., Kuszewski, J., Nilges, M., Pannu, N. S., Read, R. J., Rice, L. M., Simonson, T., and Warren, G. L. (1998) *Acta Crystallogr. D*, In press.
24. Jones, A. (1978) *J. Appl. Crystallogr. 11*, 268−272.
25. Palleros, D. R., Reid, K. L., Shi, L., Welch, W. J., and Fink, A. L. (1993) *Nature 365*, 664−666.
26. O'Brien, M. C., and McKay, D. B. (1995) *J. Biol. Chem. 270*, 2247−2250.
27. Flaherty, K. M., McKay, D. B., Kabsch, W., and Holmes, K. C. (1991) *Proc. Natl. Acad. Sci. U.S.A. 88*, 5041−5045.
28. Kraulis, P. (1991) *J. Appl. Crystallogr. 24*, 946−950.

BI981510X